OPO OPHTHALMIC & PHYSIOLOGICAL OPTICS
THE JOURNAL OF THE COLLEGE OF OPTOMETRISTS

Ophthalmic & Physiological Optics ISSN 0275-5408

Improved fixation quality provided by a Bessel beacon in an adaptive optics system

Andrew J Lambert[1], Elizabeth M Daly[2] and Christopher J Dainty[2,3]

[1]School of Engineering and Information Technology, The University of New South Wales, Australian Defence Force Academy, Canberra, Australian Capital Territory, Australia, [2]Applied Optics, School of Physics, National University of Ireland Galway, Galway, Ireland, and [3]Blackett Laboratory, Imperial College, London, UK

Citation information: Lambert AJ, Daly EM & Dainty CJ. Improved fixation quality provided by a Bessel beacon in an adaptive optics system. *Ophthalmic Physiol Opt* 2013. doi: 10.1111/opo.12071

Keywords: adaptive optics, Bessel beam, fixation, retinal imaging

Correspondence: Andrew Lambert
E-mail address: a.lambert@adfa.edu.au

Received: 1 November 2012; Accepted: 9 April 2013

Abstract

Purpose: We investigate whether a structured probe beam that creates the beacon for use in a retinal imaging adaptive optics system can provide useful side effects. In particular we investigate whether a Bessel beam that is seen by the subject as a set of concentric rings has a dampening effect on fixation variations of the subject under observation. This calming effect would allow longer periods of observation, particularly for patients with abnormal fixation.
Method: An experimental adaptive optics system developed for retinal imaging is used to monitor the fluctuations in aberrations for artificial and human subjects. The probe beam is alternated between a traditional beacon and one provided by a Bessel beam created by SLM.
Results: Time-frequency analysis is used to indicate the differences in power and time variation during fixation depending on whether the Bessel beam or the traditional beacon is employed. Comparison is made with the response for an artificial eye to discount systemic variations.
Conclusion: Significant evidence is accrued to indicate the reduced fluctuations in fixation when the Bessel beam is employed to create the beacon.

Introduction

Traditionally, adaptive optics (AO) systems for the human eye have used a single beacon which enters the eye as a narrow beam and forms a relatively large spot on the retina. Information about the eye's aberrations can be obtained by examining how light from this spot travels back out through the full ocular pupil to the wavefront sensor (WFS). The WFS in turn can provide feedback to a correcting element to compensate for the static and dynamic ocular aberrations and allow, for example, high-resolution retinal imaging to take place.[1] In this simplest implementation the probe beam itself is distorted by the aberrations as it travels to the retina, while variable scatter from the retina distorts its shape and quality. One approach to counter these incoming aberrations is to pass the probe through the AO correction system before it enters the eye, resulting in a tight diffraction-limited spot on the retina when the AO loop is closed. However, the very weak return from the retina in flood-illuminated retinal imaging systems may then be swamped by reflections of the probe from various optical surfaces. The shape and quality of the probe beam on the retina may also become an issue if this probe is being used as a medical beam or to guide a surgical procedure.

We are investigating a new type of probe beam in order to better control the quality of scatter from the retina, and be less affected by aberrations on the path into the eye than by the traditional solution where we can exert control over its focus depth, and one which subjects can fixate upon in a more stable way. We believe that a Bessel beam employed as the probe may provide some of these desirable qualities.[2,3]

In this paper we describe our experiments which observe the effects of using the Bessel beam on fixation by the subject. The beam in our case is visible, but even infrared beams are apparent to the human subject. To ensure correction by the AO system is for the same isoplanatic patch as the retinal field of interest or surgical site the beacon

needs to be placed close by, in which case the beacon itself could be the fixation target.

We have observed that subjects presented with a Bessel beam, which forms a set of annular rings on the retina, were more easily positioned, and in some cases can guide themselves onto the best centre for retinal observation. This paper investigates this observation, using the wavefront reconstruction within the AO system as evidence of its validity. Such knowledge may aid both diagnosis of, or better ophthalmic examination of, subjects who have fixation difficulties. As these patients are the most likely to require ophthalmic examination, any ability to detect or stabilise temporal variation in physiology would be of great benefit to clinicians. For example, patients with Down and Williams syndrome,[4] Parkinson's and Hodgkin's disease, or toddlers,[5] or amblyopia,[6] juvenile[7] and age related macular degeneration[8–10] patients are known to exhibit abnormal fixation.[11] These are seen as ocular flutter, micro-saccades, micro-tremors[12] and Nystagmus.[11] Coarse evaluation of these is possible through pupil tracking,[13,14] fundus imaging and alignment,[8,9] but a finer measure would be an advantage in diagnosis.

Diseases in patients may be detected at early stages by retinal examination. AO is typically used for pathology after initial detection, but patient groups who are unable to fixate for enough time are difficult to examine, and may put too high a demand on the AO feedback loop as large variations in tip and tilt are not easily compensated by current deformable mirrors. Hence the ability to use the beacon in such a way that it effectively calms the fixation would be clearly advantageous.

This investigation does expose these properties, and to our knowledge has not yet been utilised in AO systems. Passive (non AO) fixation targets may well have a similar effect,[15,16] as is evidenced by a substantial body of work that underlies even the laser safety standards.[17] Here the quantity, T_2, used in these standards to embody the typical time that an unconstrained eye can remain stable, is extended for an extended source or image formed on the retina. A recent work reports the unique effect a 'bull's-eye' target has on stability of vision, when compared to other extended targets.[18]

The use of the illumination within the AO system itself would seem an ideal approach to extending the fixation time, and for evaluating the normal and abnormal deviations from fixation-like ocular flutter, micro-saccades, and pathological causes. The added benefits to controlling the illumination are described elsewhere.[2]

Method

Apparatus

The experiment was performed using an adaptive optics system based upon the pyramid wavefront sensor (PWS), which has been described in detail elsewhere.[2,19] A schematic is shown in *Figure 1*. The system is designed to measure and/or correct aberrations in the human eye in-vivo at 675 nm. A range of spatial sampling options are available depending upon the wavefront sensor CCD pixel binning setting, but all of this work was carried out at binning setting B4,[19] corresponding to 24 samples of the wavefront across the 6 mm measurement pupil. The speed of the system is nominally 63 frames-per-second at this level of spatial resolution. The PWS allows for different dynamic range/sensitivity settings depending upon the aberrations of the subject under test; for this work we used two settings, referred to as M10 and M15. The corresponding root-mean-square (RMS) wavefront reconstruction errors were 30 and 39 nm respectively. As the primary use for this system is to image the retina using green light, the position of the retinal imaging camera (Andor Luca EM247 Mono; www.andor.com) is optimised after a dichroic beamsplitter to maximise collection of 532 nm light. Unfortunately this means that relatively long exposures (>50 ms) were required to capture images of the beacon (either conventional or modified) on the retina which is in the red at 675 nm. The transverse magnification from retina to science camera is ×6.7 for an artificial eye and ×6.3 for an emmetropic human eye. The Bessel beacon required for the work described in this paper was created using a spatial light modulator (SLM) placed in a conjugate pupil plane, enabling application of appropriate phase masks to the incoming light. This process was described in detail by Lambert *et al.*[2] Here we adopt the terminology for the probe beam formed with the SLM with no spatial phase, $\beta = 0$ pixel^{-1}, as 'Flat', and with a radial phase of $\beta = 0.1$ pixel^{-1}, as 'Bessel'.

Measurements

Measurements were carried out on the right eyes of two volunteers: Subject A (33 years) is very slightly hyperopic (>0.5 D) and Subject B (46 years) is myopic with a −1.5 D prescription. All focus errors were corrected with the system Badal before storage of any wavefront data. Subjects were dilated using 1% Tropicamide and stabilised to the system using a bite bar. Each subject was presented with a Bessel beacon and asked to fixate upon the centre of the resulting concentric rings which are visible in the retinal image plane. A chirp coefficient added to the applied phase mask allows control over the axial location of best focus; this was varied to find the setting which gave the sharpest image of the Bessel rings for the subject. Approximately 15 s of open loop PWS data were stored. The subject was then presented with the Flat beacon, and another 15s of open loop data were stored. This was repeated three times for each subject. For these trials the laser powers measured

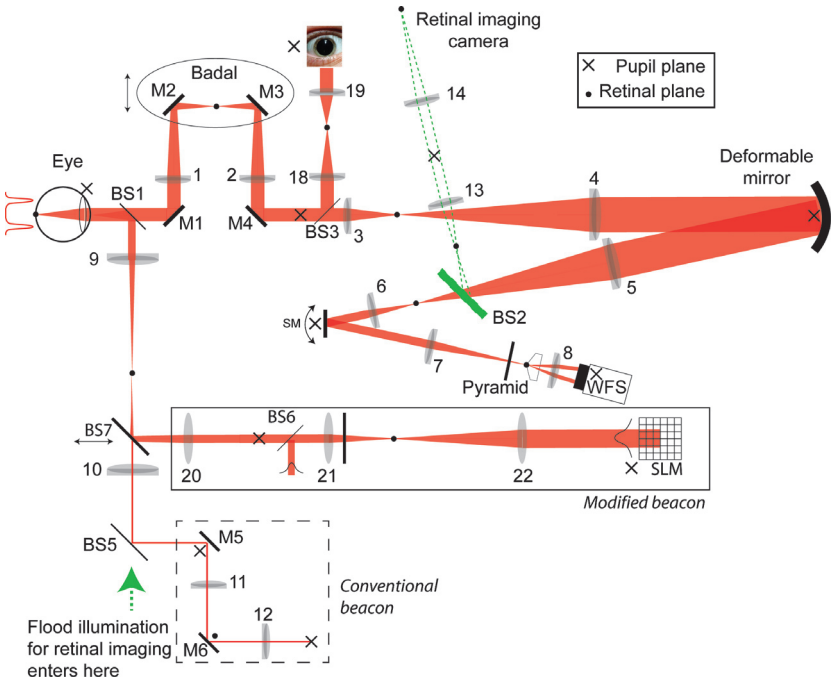

Figure 1. Schematic of the experimental adaptive optics (AO) system used to perform fixation measurements. The conventional beacon for AO is indicated by the dashed box, while the modified beacon, shaped by the spatial light modulator and used in this work, is indicated by the solid box. Lenses in the setup are numbered 1–22; flat mirrors are denoted M and beamsplitters BS; DM is the deformable mirror; SM is the steering mirror used for range/sensitivity adjust in the PWS; WFS is the wavefront sensing camera; the pupil plane and its conjugates are marked with an *x*; the retinal plane and its conjugates are marked with a •. A pupil alignment camera is located after lens 19, while the retinal imaging camera is located after lens 14. The AO system operates in the red at 675 nm, while the optics for retinal imaging are optimized for green light at 532 nm.

at the cornea were 2 μW for Subject A and 3 μW for Subject B, both over an order of magnitude lower than the maximum permissible exposure at the illumination wavelength of 675 nm (intrabeam viewing).[17] This work has received ethical approval from the National University of Ireland Galway Research Ethics Committee. All measurements were repeated using an artificial eye for reference.

Results

The beacons visible to each subject depending upon the SLM settings are shown in *Figure 2*. These images were obtained by placing a small monochrome camera (Lumenera Lu175M; www.lumenera.com) at the position of the retina behind a lens of focal length 40 mm. Part (a) shows the concentric rings that the subject sees for a Bessel beacon. The extra rings visible here are due to non-linearities in optical rendering of the desired phase mask within the SLM. Part (b) shows the spot from the Flat beacon. Both the Bessel and Flat beacons occupy the full entrance pupil (6 mm), both having uniform magnitude across the SLM, just differing by virtue of the Bessel phase.[2] The wide pupil results in a very tight point spread function on the retina. In contrast, the conventional beacon used in the AO system has a beam diameter at the pupil of just 1 mm, resulting in an aberration-free point spread function (peak to first zero) of 14 μm.

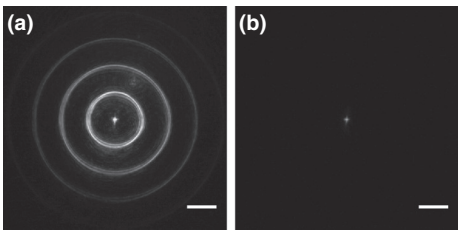

Figure 2. Images of the modified beacon as it appears to the subjects. Part (a) shows the beacon resulting on application of a phase mask at the spatial light modulator with Bessel coefficient $\beta = 0.1$ pixel^{-1}; part (b) shows the narrow beacon that results when $\beta = 0$ pixel^{-1}. Exposure times were 4 ms (a) and 2 ms (b) respectively. Scale bars correspond to 200 μm (5 mrad).

Bessel images

Figure 3 shows images of these beacons as captured by the retinal imaging camera located after the dichroic beamsplitter BS2. The top row corresponds to the Flat beacon, while

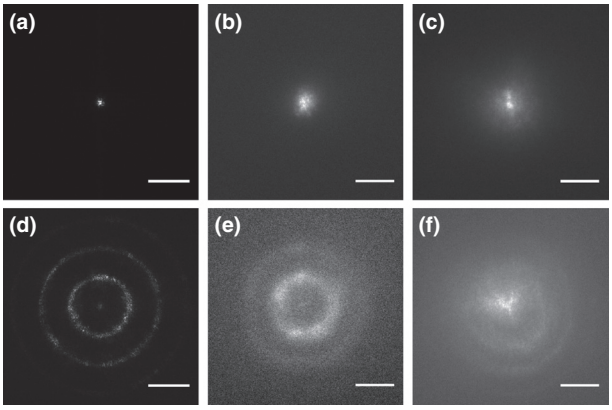

Figure 3. Images of the modified beacon obtained through the adaptive optics system by the retinal imaging camera. The top row of this figure corresponds to $\beta = 0$ pixel^{-1}, while the bottom row corresponds to $\beta = 0.1$ pixel^{-1}. Parts (a) and (d) are obtained from an artificial eye with exposure times of 0.5 and 10 ms respectively. The Bessel structure is clear with a number of concentric rings easily visible. Data from Subject A are shown in (b) and (e), and from Subject B in (c) and (f). Exposure times were longer (50 ms) for the real eyes, and each image shown here was obtained by registration of 10 individual frames. Scale bars correspond to 100 μm (5.8 mrad assuming $f = 17$ mm).

the bottom row images were obtained from the Bessel beacon. Parts (a) and (d) show the beacon as it appears on an artificial retina, parts (b) and (e) show results for Subject A, and parts (c) and (f) are the images obtained from Subject B. In all cases the images shown here are the result of registering 10 frames after subtracting a camera bias frame from each. Exposure times for the subjects were 50 ms, while those for the artificial eye were 10 ms (Bessel) and 0.5 ms (Flat). The adaptive optics loop was not running while these images were obtained so subject aberrations were not corrected; the deformable mirror was left in the bias position. The images shown are consistent with experimental conditions for the fixation quality trials. Movement of the subjects within the 50 ms frame time undoubtedly contributes to the blurring of the Bessel structure, as do the uncorrected subject aberrations, e.g., the myopia of subject B that is not fully corrected by the Badal stage resulting in a much wider point spread function than subject A. Scattering contributes to the large halo. For completeness the tip-tilt removed RMS wavefront error (averaged over three 15 s recordings) for each subject and beacon is given in *Table 1*.

Time variation of Zernike terms

For fixation trials, the open loop data stored by the PWS were in the form of raw wavefront gradients. These were post processed to expand the wavefront in terms of Zernike polynomials (36 terms), where the OSA standard for labelling of the coefficients is used.[20] *Figure 4* shows the reconstructed Zernike *y*-tip (J1) and *x*-tilt (J2) terms for Subject A during a single trial of fixation quality.

Table 1. The RMS wavefront error (tip-tilt reduced) for each test subject and beacon

	Bessel, μm (β = 0.1)	**Flat, μm (β = 0)**
Subject A	0.243	0.331
Subject B	0.214	0.248
Artificial eye	0.194	0.209

Power spectral density

Initially, a spectral analysis of the time-varying RMS total wavefront error was performed for each subject, after removal of blinks by manual exclusion of certain time periods from the RMS traces. This analysis was based upon the Lomb-Scargle periodogram for non-uniformly spaced data.[21] We found that the Power Spectral Density (PSD) measured for real eyes had higher magnitude than that measured for an artificial eye at the same experimental settings, confirming that the energy measured was indeed due to the dynamic aberrations of the subjects. We also analysed the PSD of Zernike tip and tilt terms individually, as shown in *Figure 5* for both subjects. This figure shows log-

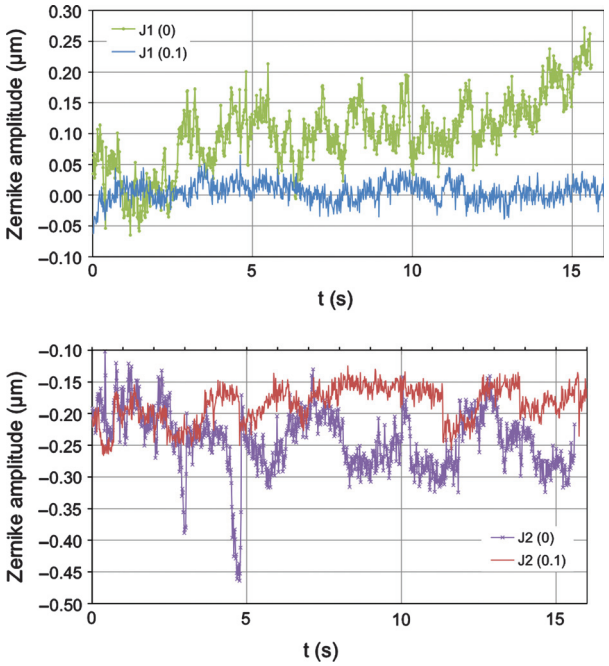

Figure 4. Reconstructed Zernike y tip (J1) and x tilt (J2) terms for Subject A during a single trial of fixation quality. The value of β is indicated in brackets in the figure legend for each curve. Solid lines with crosses: $\beta = 0$; dashed line: $\beta = 0.1$ pixel^{-1}.

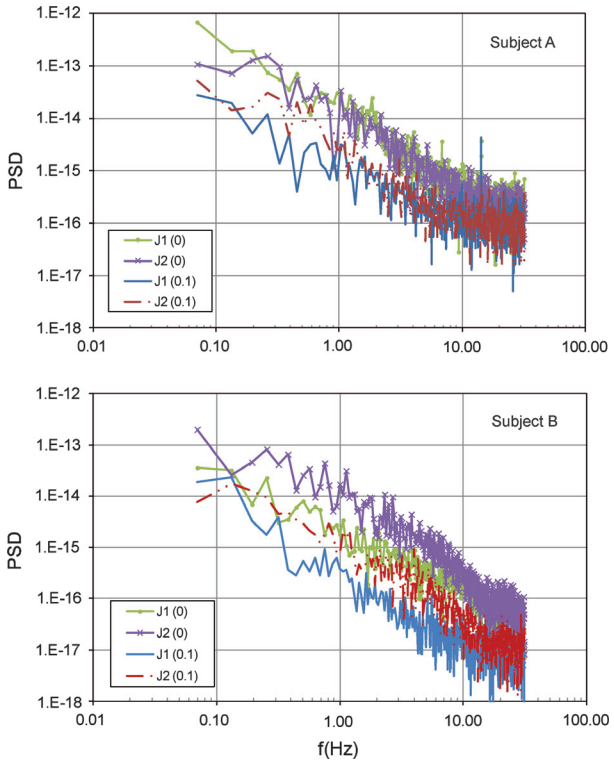

Figure 5. Power spectral density (PSD) of individual Zernike terms, averaged over three trials, for Subjects A and B. Solid line with circles: J1 at $\beta = 0$; dashed line with crosses: J2 at $\beta = 0$; solid line: J1 at $\beta = 0.1$; dashed line: J2 at $\beta = 0.1$ pixel^{-1}. The small peak in some curves for Subject A at around 14 Hz is probably due to aliasing of the SM modulation (100 Hz) sampled by the wavefront sensor at 63 Hz. It was not visible for Subject B, because this data were taken at a smaller range setting, therefore smaller amplitude of modulation of the SM applied voltage.

log plots of PSD for J1 and J2 Zernike terms, for Flat and Bessel beacons. Each curve in the figure is an average over the three trials run with each beacon type.

Time-frequency analysis

To observe the temporal fluctuations in the Zernike coefficients of the wavefront reconstruction we need to use time-frequency analysis. The PSD collates power at each frequency over the entire observation period, but we expect this power to vary in its distribution over short periods of time. Similarly examination of the sampled time signal shows statistical variance, but it is difficult to ascertain the rapidity of response that shows as frequency content. We expect the causes of fluctuation to be non-stationary.

The Matlab function *specgram* may be used to divide the time signal into portions, from which the pseudo-instantaneous frequency response is obtained using the Fast Fourier Transform (FFT) over 256 frequency bins. Conditioning of these portions is obtained by windowing with a Hanning profile over each collection of 128 data points. A typical colour coded plot of power vs time and frequency is shown in *Figure 6*, for the J2 and in *Figure 7* for the J1 Zernike coefficients. Majority low frequency contribution to the plots, with little or no time variation in that power, would indicate a highly stable fixation. Absence or reduced power at lower frequency, with accompanying increase in power at higher frequencies would indicate much activity in either the wavefront estimation or the subject's optical system. Temporal variation any of this would indicate non-stationarity, such a bursts associated with saccades.

To identify the limits of this analysis and for a control observation, we present the same plots from an artificial eye illuminated with a Bessel (left) and Flat (right) beacon. The latter provides a more traditional tight spot on the retina, modified by the specific aberrations of the subject. These benchmark the noise floor and the degree to which the beacon shape interacts with the estimation, in the top row Subsequent rows illustrate the response by two subjects respectively.

We present a simpler visualisation of the activity over time and frequency. For each Zernike coefficient, we identify the maximum power in any of the six spectrograms in *Figures 6 and* 7, and ratio each of them to this value, x_{max}. By repeatedly decreasing a threshold by 1 dB, and counting the fraction of pixels above that level, we form the cumulative variation with threshold (x-axis) as shown in *Figure 8*, for each of (a) J1 (b) J2 (c) J4 (d) J7 and (e) J8 coefficients. The curves are independent of the actual power in that Zernike term, but we assume a dominant frequency is present in the spectrogram. The curves rise from the x-axis at different locations, related to the relative maximum power in each spectrogram. Appropriate comparison is therefore the spacing between the flat and Bessel curves for each subject, not the comparison between subjects or to the artificial eye. Curves closer to the left indicate significant activity during the observation. Interpretation of differences at the low power levels associated with the artificial eye to the right should be conducted with caution.

Discussion

Time variation of Zernike terms

Figure 4 shows typical time sequences for the Zernike coefficients, and illustrates that there is significantly more power in the coefficients J1 and J2 for the Flat compared with the Bessel beacon, even to the extent in J2 for the Flat beacon, of exhibiting saccade type responses. Note that the offset between traces is not so important, as it indicates the subjects quiescent alignment with respect to the system, but the wander for the Flat beacon over time in the J1 tip axis indicates subject specific variation.

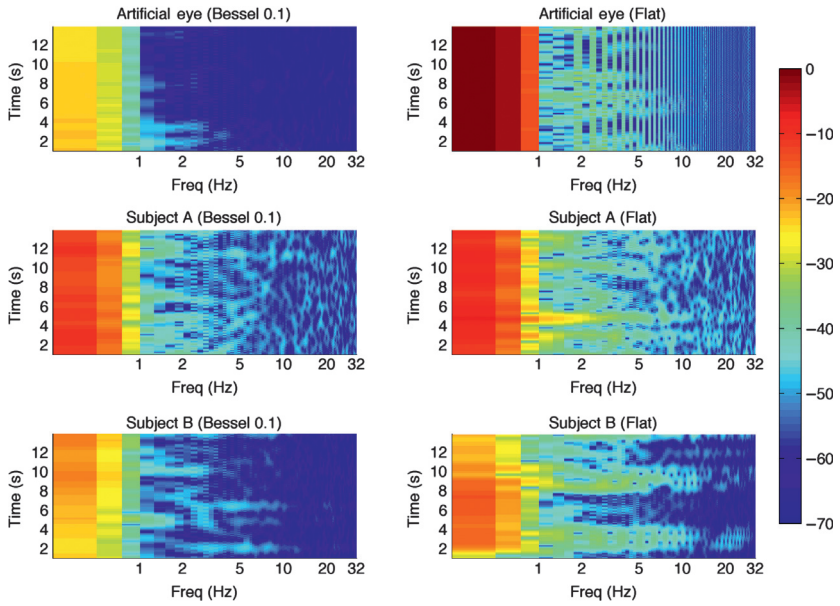

Figure 6. The time-frequency analysis of the contribution of the tilt (J2) Zernike to the reconstructed wavefronts, is shown for (left) Bessel $\beta = 0.1$ pixel^{-1} and (right) Flat spatial light modulator $\beta = 0$ pixel^{-1} probes. (top row) Artificial eye, (centre row) Subject A, and (bottom row) Subject B.

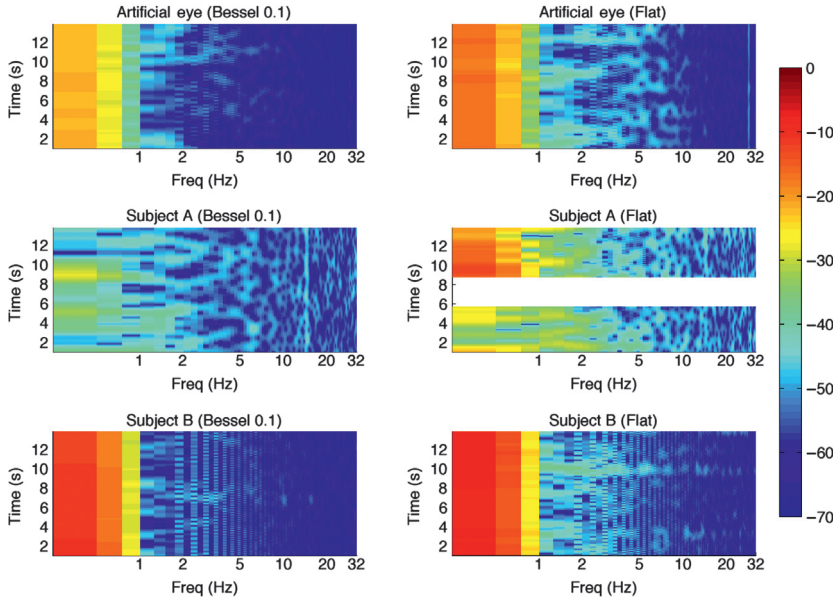

Figure 7. The time-frequency analysis of the contribution of the tip (J1) Zernike to the reconstructed wavefronts, is shown for (left) Bessel $\beta = 0.1$ pixel^{-1} and (right) Flat spatial light modulator $\beta = 0$ pixel^{-1} probes. (top row) Artificial eye, (centre row) Subject A, and (bottom row) Subject B.

Power spectral density

The PSD for both subjects are plotted for tip and tilt signals for both the Bessel and Flat beacons, for comparison in *Figure 5*. The PSD curves for each case are separated vertically, in a similar way to the observations of the artificial eye. Close observation of the PSD in both subjects, shows another type of separation between the J1 and J2 curves of the Bessel (blue-red) and Flat (green-magenta) beacons, between approximately 0.3 and 3 Hz. Here the Bessel PSD

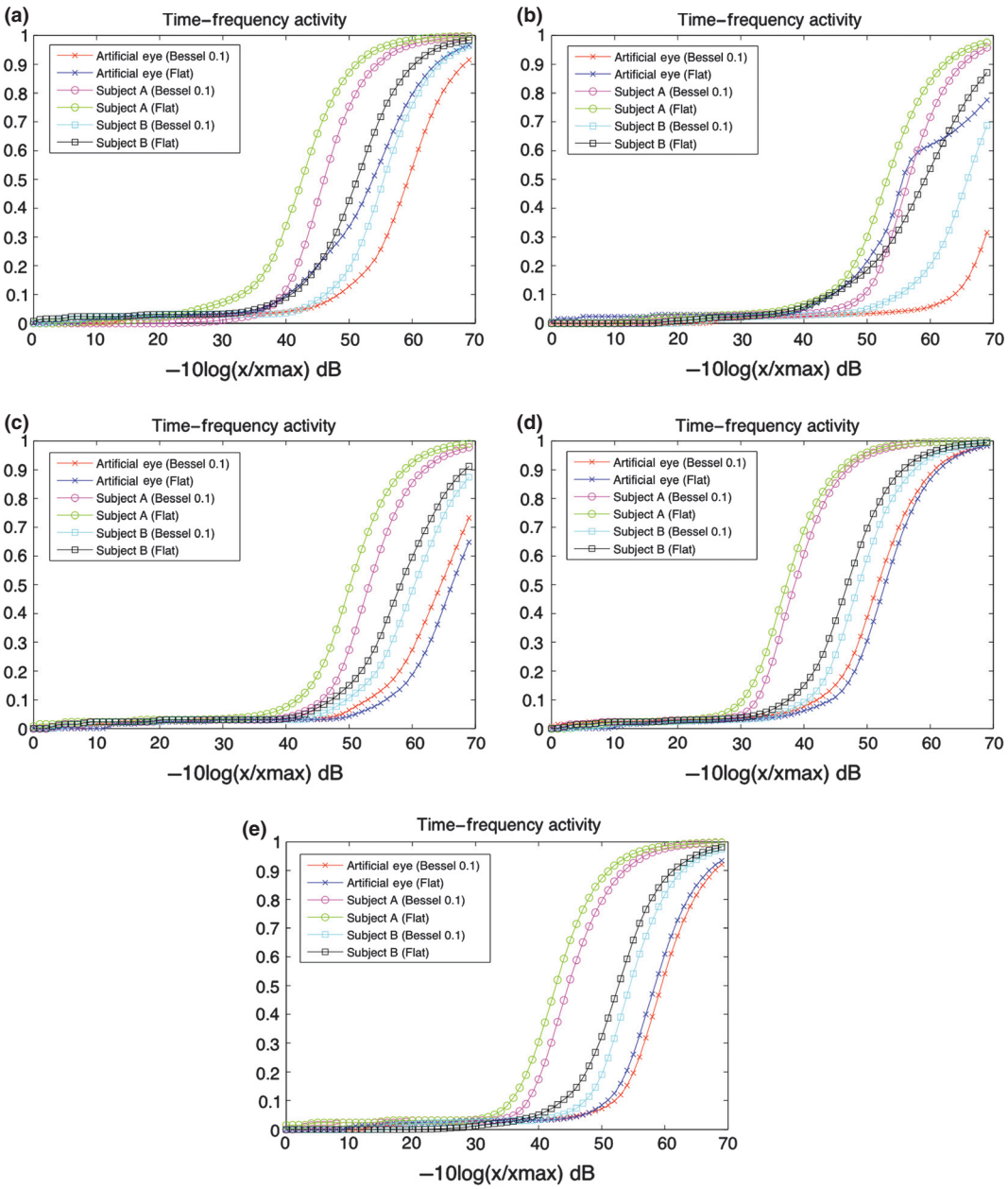

Figure 8. Measures of the activity in the time-frequency domain for each of the (a) J1, (b) J2, (c) J4 (d) J7, and (e) J8 Zernike contributions to the estimated wavefront. Curves are shown for cumulative power above the threshold (*x*-axis) in the cases of two subjects and the artificial eye, for $\beta = 0$ (Flat spatial light modulator) and $\beta = 0.1$ pixel^{-1} (Bessel).

have a slight plateau rather than following the trend shown for the Flat beacon. This would indicate the power in the Bessel response is confined to very low frequency, whereas the Flat beacon suffers more variation, more frequently. This could be loosely construed as quiescence with the Bessel. In the presence of the Bessel beacon a detrending for both subjects between J2 (tilt-*x*) and J1 (tip-*y*) PSD, is noticed in the range 0.1–1 Hz. This might evidence that there is more variation naturally in the x-direction. It is not apparent with the Flat beacon, due to the other variations dominating, whereas the dampening effect of the Bessel makes it subtly visible.

Time-frequency analysis

The question of whether the fluctuation in the coefficients is caused by noise in the process that may be coloured by the type of beacon, or because of subject physiology, is

answered using time-frequency analysis. The time-frequency plots shown in *Figures 6 and 7* are for the tilt (J2) and tip (J1) coefficients respectively. By comparison the PSD shown in *Figure 5*, is the summation of these plots in the vertical direction, and does not show the bursting phenomena. The same sets for J4, J7 and J8 (not shown) exhibit much less fluctuation, as also evidenced in *Figure 8c–e*. For each subject, the time-frequency variations produce similar effects in each of the three runs. The top row of each figure is the benchmark for the PWS estimation using an artificial eye, and serves to indicate the inherent noise floor for each probe beam. As the artificial eye is fixed we would expect any variation, of which there is clearly very little, to be systemic to the PWS estimation, or within the numerical accuracy. Note the large range present in both, and the structural artifacts in the rightmost picture are more than 30 dB below the main power level. The leftmost start at a lower power, but exhibit a similar range. Both show little time variation to the power distribution over frequency. However, for the central and bottom rows the variation is evident over both time and frequency. Variation in *Figure 6*, is most profound for the Flat beacon, both in the lower frequency power fluctuations, and also in burst over a significant frequency range, which we attribute to micro-saccades. Lesser activity for the Bessel beacon, is also coupled with less bursting, which we argue indicates sustained fixation.

The same trends are evident in *Figure 7*, where the Bessel exhibits less variation. The light blue vertical line feature evident in some plots, is an alias of the pyramid modulation procedure at 100 Hz. For subject A (centre row) a blink has occurred during recording as evidenced by the blank region, and serves to delineate the variation in power before and after the blink. For example consider the change in colour scheme at low frequency to bright red just after the blink, and compacting of the frequency compared with before the blink. This indicates a renewed fixation even for the Flat beacon. On the same line the apparent variation for the Bessel is more perhaps because the power at lowest frequencies is substantially smaller by comparison, indicating the subject is centred relative to the optic axis to start. The variation in power in this case at low frequency is not accompanied by a burst of higher frequencies as seen in the saccade cases.

It is fair to say that in all the cases we recorded (two shown), that the Bessel shows much less temporal and frequency range variation, indicating a more stable subject.

The power in the leftmost columns within each plot of *Figures 6 and* 7, decreases to the right.

Interestingly, time-frequency plots for the defocus J4 show extremely small variation regardless of the beacon type or subject. The Bessel in the artificial eye shows slightly higher overall power because of the minor confusion the annulus point spread function create in the PWS, appearing like a defocus itself.[2] The lack of variation can be explained because both subjects are cyclopleged, so while they can exhibit whole eye tip and tilt, it is difficult to get variation in accomodation response associated with change in defocus. Indeed we believe this is also why there is not a more defined or regular bursting. We have observed such in non-cyclopleged subject, as well as variation in pupil dilation at the PWS. We will report on developments for non-cyclopleged subjects elsewhere, but in our observations the use of the Bessel probe has a similar dampening effect on the fixation to that shown here.

We sought a simple visualisation of the time-frequency activity to draw conclusions about fixation stability across a range of aberrations. *Figure 8* shows these cumulative curves, where a curve to the left shows significantly more variation or activity than curves farther to the right. Curves that grow to the right of the 40 dB threshold should be considered inconsequentual as they are close to the inherent noise of the process.

Analysis of these curves for both subjects shows that the Flat beacon results in more activity than the Bessel in all cases. The sets in *Figure* 8 are for J1 (tip), J2 (tilt), J4 (defocus), J7 (coma in y), and J8 (coma in x). In the cases of J2 and J8 there is significant difference between Flat and Bessel beacons for both subjects, while the other coefficients and the artificial eye observations show little difference based on the type of beacon. Note some curves hug the x-axis to a lower power than the others in the same set, and these indicate the power being confined to extremely low frequencies with little variation. This is the case for example in *Figure 8a* for the Bessel response of subject A (magenta circle trace), where this trace shows more activity when seen in *Figure 7* (left, centre row) than the other in that set, but clearly with a higher noise floor than the others. The normalisation of the curves to the maximum power in any observation, which can be low, or be little different to the power at other frequencies can distort these curves. It is assumed the power distribution between spectrograms be similar between types of probe for each subject, in which case the two curves for each subject can be compared. The curves should not be compared between subjects, nor if the spectrogram shows little structure.

Conclusion

We have performed time-frequency analysis of variation within the Zernike coefficients and determined that a Bessel beacon could aid fixation studies by reducing the variance associated with the traditional beacon, even for cyclopleged subjects. Reduction in activity is noticed primarily in the

aberrations associated with the *x*-axis, e.g., J2 and J8. Potential gains to clinical use in disease diagnosis could arise from this type of probe beam in an AO instrument. Whether the gains are a consequence of the Bessel beam or are similar to that found with a 'bull's-eye' extended target[18] is an outstanding question, but properties possessed by a Bessel beam may provide additional significance beyond stabilising vision.

Disclosure

The authors report no conflicts of interest and have no proprietary interest in any of the materials mentioned in this article.

Acknowledgements

This work was supported by the Australian Research Council grant DP110102018, and Science Foundation Ireland grant SFI/07/IN.1/1906. The authors wish to thank Dr. Conor Leahy of Applied Optics for Matlab code for calculation of the PSD.

References

1. Liang J, Williams DR & Miller DT. Supernormal vision and high-resolution retinal imaging through adaptive optics. *J Opt Soc Am A* 1997; 14: 2884–2892.
2. Lambert AJ, Daly EM & Dainty JC. Supplementary active optics for illumination within an adaptive optics system. *J Mod Optic* 2011; 58: 1716–1728.
3. Dyson J. Circular and spiral diffraction gratings. *Proc Roy Soc Lond A* 1958; 248: 93–106.
4. Brown JH, Johnson MH, Paterson SJ, Gilmore R, Longhi E & Karmiloff-Smith A. Spatial representation and attention in toddlers with Williams syndrome and Down syndrome. *Neuropsychologia* 2003; 41: 1037–1046.
5. Dinkin MJ & Rizzo JF III. Abnormal eye movements in children. *Int Ophthamol Clin* 2008; 48–2: 95–133.
6. González EG, Wong AM, Niechwiej-Szwedo E, Tarita-Nistor L & Steinbach MJ. Eye position stability in amblyopia and in normal binocular vision. *Invest Ophthalmol Vis Sci* 2012; 53–9: 5386–5394.
7. Macedo AF, Nascimento SM, Gomes AO & Puga AT. Fixation in patients with juvenile macular disease. *Optom Vis Sci* 2007; 84–9: 852–858.
8. Amore FM, Fasciani R, Silvestri V *et al.* Relationship between fixation stability measured with MP-1 and reading performance. *Ophthalmic Physiol Opt* 2013; doi:10.1111/opo.12048.
9. Elsner AE, Petrig BL, Papay JA, Kollbaum EJ, Clark CA & Muller MS. Fixation stability and scotoma mapping for patients with low vision. *Optom Vis Sci* 2013; 90–2: 164–173.
10. Sivaprasad S, Pearce E & Chong V. Quality of fixation in eyes with neovascular age-related macular degeneration treated with ranibizumab. *Eye (Lond)* 2011; 25–12: 1612–1616.
11. Ditchburn RW & Ginsborg BL. Involuntary eye movements during fixation. *J Physiol Lond* 1953; 119: 1–17.
12. Ryle JP, Al-Kalbanid M, Gopinathan U, Boyle G, Caokley D & Sheridan JT. Speckle interferometric sensor to measure low-amplitude high frequency Ocular Microtremor (OMT). *P Soc Photo opt Inst* 2009; 7429: 74290J-1–74290J12.
13. Wallis G. The temporal and spatial limits of compensation for fixational eye movements. *Vision Res* 2006; 46: 2848–2858.
14. Dimigen O, Valsecchi M, Sommer W & Kliegl R. Human microsaccade-related visual brain responses. *J Neurosci* 2009; 29–39: 12321–12331.
15. Iglesias I, Ragazzoni R, Yves J & Artal P. Extended source pyramid wave-front sensor for the human eye. *Opt Express* 2002; 10–9: 419–428.
16. Garcia-Diaz A, Lebora´n V, Fdez-Vidal XR & Pardo XM. On the relationship between optical variability, visual saliency, and eye fixations: a computational approach. *J Vis* 2012; 12–6: 1–22.
17. British-Adopted European Standard BS EN 60825-1:2007 *Safety of Laser Products- Part 1: Equipment Classification and Requirements* (British Standards Institution, 2009). See also AS/NZS IEC 60825.1:2011.
18. Thaler L, Schütz AC, Goodale MA & Gegenfurtner KR. What is the best fixation target? The effect of target shape on stability of fixational eye movements. *Vision Res* 2013; 76: 31–42.
19. Daly EM & Dainty C. Ophthalmic wavefront measurements using a versatile pyramid sensor. *Appl Opt* 2010; 49: G67–G77.
20. Thibos LN, Applegate RA, Schwiegerling JT & Webb R. Vision Science and its Applications. In: Trends in Optics and Photonics Series (Lakshminarayanan V, editor), Vol. 35, Optical Society of America: Washington DC, 2000; pp. 233–244.
21. Scargle JD. Studies in astronomical time series analysis. II. Statistical aspects of spectral analysis of unevenly spaced data. *Astrophys J* 1982; 263: 835–853.

